Available online at www.sciencedirect.com
ScienceDirect
Journal of Catalysis 253 (2008) 212–220
JOURNAL OF CATALYSIS
www.elsevier.com/locate/jcat

A theoretical investigation into the thiophene-cracking mechanism over pure Brønsted acidic zeolites

Bingrui Li [a], Wenping Guo [a,b], Shuping Yuan [b,c], Jia Hu [a,b], Jianguo Wang [b,*], Haijun Jiao [b,d,*]

[a] College of Chemistry and Chemical Engineering, Lanzhou University, Lanzhou 730000, China
[b] State Key Laboratory of Coal Conversion, Institute of Coal Chemistry, Chinese Academy of Sciences, P.O. Box 165, Taiyuan 030001, China
[c] Institute for Computational Science and Engineering, Laboratory of Fiber Materials and Modern Textile, The Growing Base for State Key Laboratory, Qingdao University, Qingdao 266071, China
[d] Leibniz-Institut für Katalyse e.V. an der Universität Rostock, Albert-Einstein-Strasse 29a, 18059 Rostock, Germany

Received 29 May 2007; revised 5 September 2007; accepted 8 October 2007
Available online 19 November 2007

Abstract

The mechanism of thiophene cracking catalyzed by Brønsted acidic zeolites was computed at the level of B3LYP density functional theory. It was found that this catalytic reaction involves two major steps: (1) protonation of thiophene associated with an electrophilic aromatic substitution to another thiophene in a concerted way to form 2-(2,5-dihydrothiophen-2-yl) thiophene, and (2) C–S bond dissociation in 2,5-dihydrothiophene promoted by further protonation. The intermediate, 4-mercapto-1-(thiophen-2-yl)but-2-en-1-ylium, was found to have a CH_2 group close to a C=C bond and a SH group, in agreement with the experimental findings. A strong stabilization effect of the zeolite framework on the transition states was found by embedding the 5T cluster into the larger 34T and 56T clusters. The rate-determining step is the electrophilic aromatic substitution.

Keywords: Thiophene cracking; Mechanism; Acidic zeolites; Density functional theory

1. Introduction

Due to the worldwide environmental restrictions on sulfur content in fuels, minimizing sulfur-containing organic compounds in fluidized catalytic cracking (FCC) gasoline to the greatest degree possible is desirable. Because thiophene sulfur represents a large fraction of the total sulfur content in FCC gasoline [1–4], traditionally attention has focused on thiophene hydrodesulfurization (HDS).

The conventional HDS catalysts generally consist of transition metal (e.g., M–Ni or W–Ni) sulfides dispersed over γ-alumina or acidic zeolite supports [5–7], and the HDS processes require an H_2 atmosphere, often at high pressures. Interestingly, it has been found that acidic zeolites alone also can catalyze thiophene desulfurization [8–13]. In 1975, De Angelis and Appierto [14] observed the cleavage of thiophene C–S bond and the formation of –SH groups over HY zeolites by an infrared method. Garcia and Lercher [8,9] studied thiophene adsorption on NaZSM-5, KZSM-5, and HZSM-5 and found that thiophene adsorption at a coverage of less than 1 molecule per acid site is too stable to initiate further reaction. They also found that the catalytic process could occur only at higher thiophene coverage on HZSM-5, where it undergoes intermolecular hydrogen transfer with the opening of the thiophene ring and produces thiol-like compounds containing CH_2– groups close to a double bond or to a sulfur atom. However, no such activity could be observed on NaZSM-5 and KZSM-5. Simon et al. [15] found that the C–S bond in thiophene could be broken on strong Brønsted acid sites with the formation of unsaturated thiol-like species at ambient temperatures. Welters et al. [13] studied H(x)NaY-supported metal sulfide catalysts and found that acidic zeolite supports improve thiophene HDS conversion, and that the reactions of thiophene on these zeolites cannot be explained by the conventional thiophene HDS mechanism over metal sulfide catalysts.

* Corresponding authors. Faxes: +86 351 4041153, +49 381 1281 5000.
E-mail addresses: iccjgw@sxicc.ac.cn (J. Wang), haijun.jiao@catalysis.de (H. Jiao).

0021-9517/$ – see front matter
doi:10.1016/j.jcat.2007.10.006

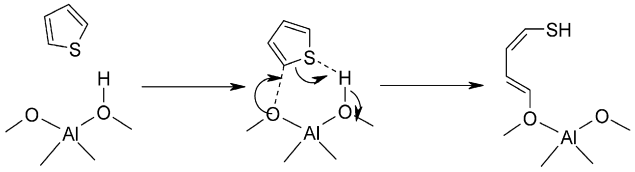

Scheme 1. Thiophene cracking mechanism proposed by Rozanska et al. [18].

As the first theoretical study on this reaction, Saintigny et al. [16] investigated thiophene desulfurization on a small $H_3SiOHAl(OH)_2OSiH_3$ (3T) cluster cut from acidic zeolites by means of a density functional theory (DFT) method, and found that the calculated activation barrier for thiophene ring cracking was about 222 kJ/mol (Scheme 1). Later, Rozanska et al. improved this approach by using a larger 4T model [17] and then a periodic model [18]. Those theoretical studies demonstrated that one of the oxygen atoms in the framework of the zeolite was the catalytic center for the reaction, whereas the Brønsted acid sites played only a limited role. However, the calculated barrier of 318 kJ/mol [18] was too high for reactions occurring at ambient temperature [8,9,12,14]. On the other hand, the proposed thiophene-cracking mechanism could not explain the formation of the observed products and the coverage effect of thiophene [8,9,12].

In 2002, Shan et al. [19] found that cracking of the C–S bond and hydrogen transfer are two major steps for thiophene and alkyl-thiophene desulfurization over USY zeolite. It was found that high temperature favors cracking, whereas low temperature favors hydrogen transfer, and that the optimal temperature for both steps is about 400 °C. Based on these findings, Shan et al. proposed an overall thiophene desulfurization reaction mechanism with the formation of a carbonium ion as an intermediate, which further reacts with a second thiophene molecule to get the ring-opening product (Scheme 2). A similar mechanism was recently proposed by Aksenov et al. [20] and Chica et al. [21,22].

Although the reaction pathways for sulfur or sulfur-free compounds proposed by Shan et al. [19], Aksenov et al. [20], and Chica et al. [21,22] can reasonably explain the experimental findings in various reactive environments, the thiophene-cracking mechanism is questionable from a theoretical standpoint. To clarify why the C–S bond in thiophene can be broken on the Brønsted acid sites at ambient temperatures, and why the thiophene ring-opening process can occur only at higher thiophene coverage, and also inspired by the suggested mechanism in Scheme 2, we proposed a different mechanism of thiophene C–S bond-cracking on Brønsted acidic zeolite on the basis of DFT calculations, in which one additional thiophene molecule is introduced near the acidic site as an assisting molecule.

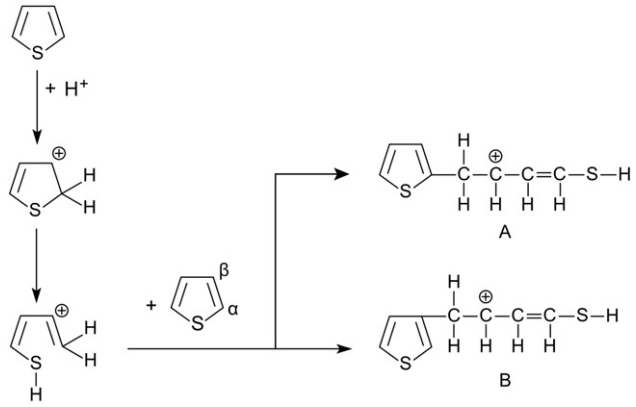

Scheme 2. Thiophene cracking mechanism proposed by Shan et al. [19].

2. Method and models

Small clusters for modeling zeolite Brønsted acid sites have been used extensively to explore reaction mechanisms. It has been proven that cluster approach is valid in predicting qualitative results in zeolite-catalyzed reactions [18]. In our work, a $Si_4AlO_4H_{13}$ cluster (5T; Fig. 1), including a complete coordination shell of oxygen around the aluminum site and representing a typical zeolite active site, was used to explore the potential energy surface. The B3LYP hybrid DFT method [23,24], the best choice for zeolite systems [25], in combination with the 6-311G(d,p) basis set, was used for full geometry optimization. Frequency calculation at the same level was carried out

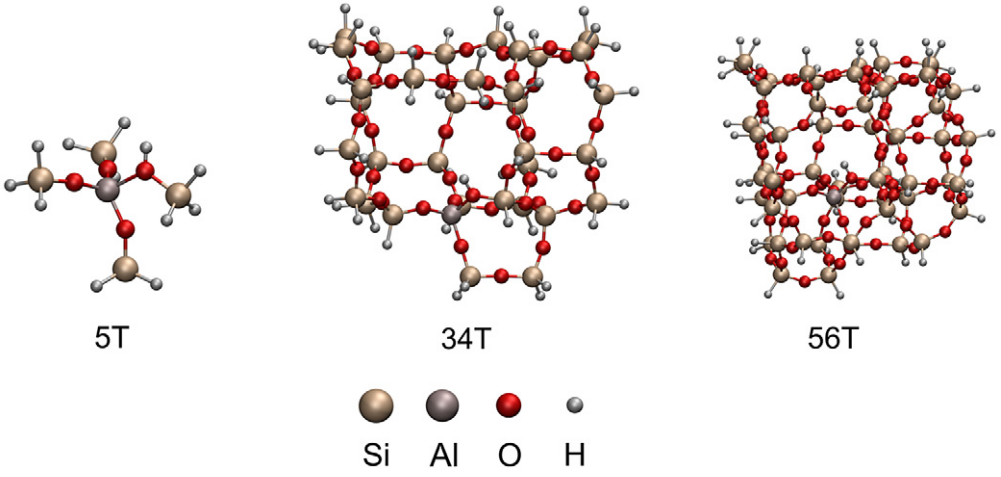

Fig. 1. 5T, 34T and 56T cluster models used in this work to represent ZSM-5 zeolite.

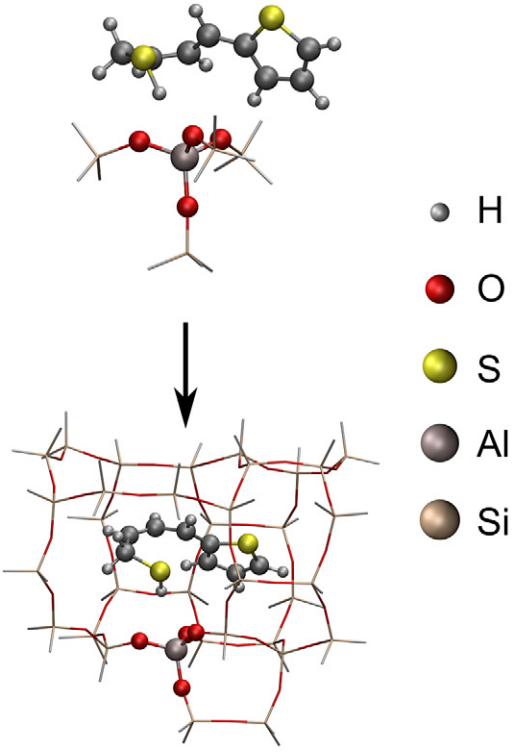

Fig. 2. Embedding scheme of 5T cluster into 34T cluster.

to verify that the stationary points thus obtained were minimum structures with only real frequencies or as transition states with only one imaginary frequency along the reaction coordinates. Zero-point energies (ZPEs) with the recommended scaling factor of 0.9877 [26] were added to the total energies of each species. Single-point energy calculations at the B3LYP/6-311 + G(2d,p) level were conducted on the optimized structures to get more accurate energies. All calculations were done using the Gaussian 03 program [27]. The molecular graphics were produced using VMD software [28].

Because long-range Coulomb interaction and some short-range interaction are not included in the 5T cluster, we used the "embedding" method of Zygmunt et al. [29] to put the 5T cluster into the larger 34T and 56T clusters to demonstrate the stabilization effect of the zeolite wall (Fig. 1). The 34T and 56T clusters, cut from the crystallographic data of HZSM-5 [30], have two characteristic channels and the intersection region of the MFI framework. ZSM-5 has 12 unique tetrahedral sites (from T1 to T12) in which one silicon atom can be substituted by an Al atom to form a Brønsted acid site. In this study, the active site was assumed to be the T12 site, because it was predicted to be the most stable Al-substituted sites [31–33], and it has been used to model the active site of ZSM-5 in many theoretical studies [34–40]. The proton is located at the intersection of the straight and sinusoidal channels, and thus is accessible to the adsorbates. In addition, the terminating hydrogen atoms are fixed at the 1.498 Å position along the lattice Si–O bonds, as determined from crystallographic data [30].

In the embedding procedure, the structure of thiophene or subsequent derivatives adsorbed on the 5T cluster was embedded in the 34T cluster (Fig. 2). Due to the large size of the

Table 1
Calculated relative energies (kJ/mol) on 5T, 34T, 56T clusters

Structures	5T[a]	5T[c]	34T[c]	56T[d]
ZOH + 2 thiophene	0.0 (0.0)[b]	0.0	0.0	0.0
MIN-1	−28.0 (−33.1)[b]	−44.0	−45.4	−47.8
TS-1	+115.1 (109.0)[b]	+80.4	+61.8	+53.1
MIN-2	−26.7 (−40.8)[b]	−63.8	−51.4	−55.0
TS-2	+76.4 (73.6)[b]	+52.4	+19.5	+11.1

[a] B3LYP/6-311 + G(2d,p)//B3LYP/6-311G(d,p) + ZPE (B3LYP/6-311G (d,p)).
[b] B3LYP/6-311 + G(2d,p)//B3LYP/6-311G(d,p).
[c] B3LYP/6-31G(d)//HF/3-21G(d).
[d] B3LYP/6-31G(d).

Table 2
Selected geometrical parameters for thiophene derivatives adsorbed on 5T framework (see Fig. 3 for the numbering system)

Thiophene derivatives	5T[a]	5T[b]
In TS-1		
C4–C5	1.99 Å	2.07 Å
H2–C5	1.10 Å	1.08 Å
C1–H1	1.09 Å	1.08 Å
In MIN-2		
C4–C5	1.50 Å	1.51 Å
S1–C4	1.89 Å	1.85 Å
C3–C4–C5–S2	142.7°	143.7°
In TS-2		
S1–C4	2.92 Å	2.79 Å
S1–H2	1.37 Å	1.33 Å
C3–C4–C5–C6	168.9°	170.5°

[a] Optimized at B3LYP/6-311G(d,p) level.
[b] Optimized at HF/3-21G(d) level.

34T cluster, we first fully optimized the structure of thiophene derivatives adsorbed on a 5T cluster at HF/3-21G(d), and then cut the optimized thiophene derivatives for embedding into the 34T cluster. In the embedded 34T cluster, only the $HAlO_4$ or AlO_4 of the 34T cluster was further partially optimized at HF/3-21G(d) (the rest kept their crystal positions), whereas the adsorbed thiophene derivatives from the HF/3-21G(d) optimization were fixed (without internal relaxation) but were allowed to adjust the relative positions (distance, angle, and torsion angle) to zeolite or the acidic center. On the basis of this partially optimized structure, we carried out single-point energy calculation at the B3LYP/6-31G(d) level. Furthermore, we expanded the embedded 34T cluster into the 56T cluster along its experimental orientation for single-point energy calculations at the B3LYP/6-31G(d) level. The computed relative energies for 5T cluster are given in Table 1, and the optimized structural parameters at both B3LYP/6-311G(d,p) and HF/3-21G(d) are compared in Table 2. The nice agreement between structure and energy validates the application of the HF/3-21G(d)-optimized geometries for the embedding scheme.

3. Results and discussion

Thiophene adsorbed on the Brønsted acid site in a 1:1 complex has been reported to be rather stable. The cracking reaction

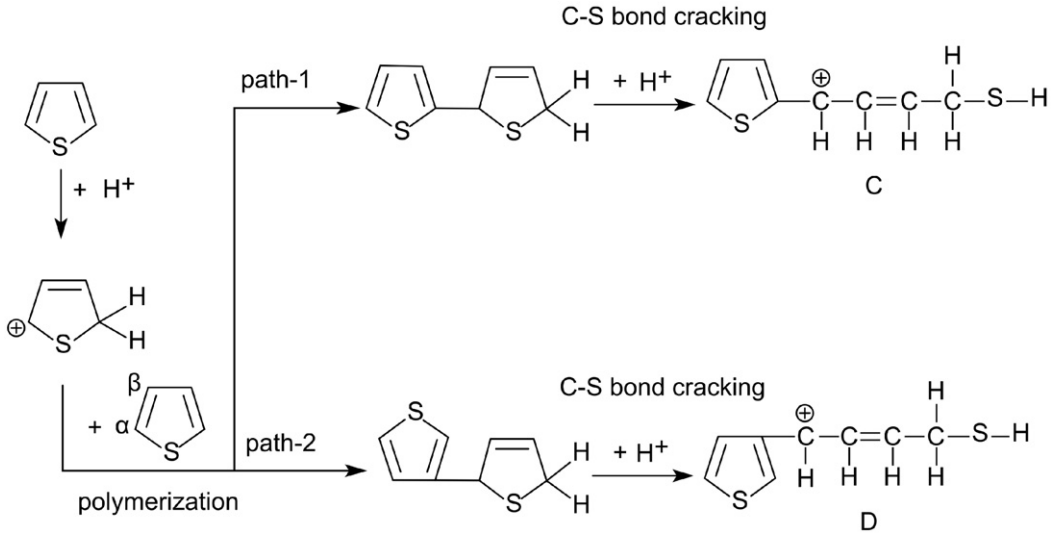

Scheme 3. Thiophene cracking mechanism proposed in this work.

occurs only at excess amounts of thiophene and immediately converts thiophene into a chemisorbed olefin–thiol-like intermediate at the zeolite wall [8,9,12]. Based on these experimental results and the proposed cracking mechanism in Scheme 2, we introduced one additional thiophene molecule to aid the cracking reaction.

The reaction path is supposed to have three steps, as shown in Scheme 3: (1) co-adsorption of two thiophene molecules in the channel of the zeolite, (2) dimerization of the co-adsorbed thiophene molecules (in a concerted way, one thiophene molecule is protonated by the acidic site and undergoes an electrophilic aromatic substitution on another thiophene molecule with its proton back to the nearby acid site), and (3) C–S bond-breaking and ring-opening of thiophene by further protonation of the same nearby acid site. Unlike the mechanism proposed by Shan et al. [19], our theoretical study shows that the C–S bond-cracking of thiophene occurs *after* the dimerization step. According to the different dimerization sites (α or β) with the assisting thiophene molecule, two possible reaction paths (paths 1 and 2) are available (Scheme 3). The α site is known to be more reactive than the β site or the sulfur center, as was also demonstrated by our calculation results; that is, protonation of the α site is favored thermodynamically over that of the β site or the sulfur center by 38.0 or 90.0 kJ/mol (Scheme 4). Therefore, the following discussion focuses on path 1. For comparison, we have computed path 2 (not competitive); these data are given in the supporting information.

3.1. Thiophene cracking over 5T cluster

The fully optimized structures of the reaction intermediates in path 1 are shown in Fig. 3, and the corresponding potential energy surface of thiophene cracking is shown in Fig. 4. The structure of **MIN-1** with two thiophene molecules co-adsorbed on the 5T cluster is shown in Fig. 3. It can be seen that one of the thiophene adopted the η^2 (C=C) mode on the Brønsted acid center; that is, its two carbon atoms had shorter distances (2.36 and 2.25 Å) to the zeolite acidic proton, whereas the thiophene

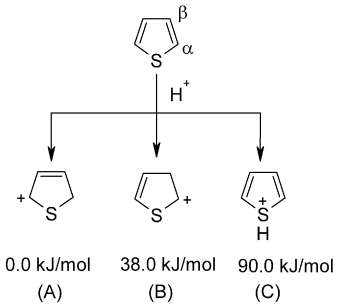

Scheme 4. Thiophene protonation energy (kJ/mol, B3LYP/6-311 + G(2d,p)// B3LYP/6-311G(d,p) + ZPE (B3LYP/6-311G(d,p))).

S atom had a longer distance (of 3.27 Å) to the zeolite acidic proton. The second thiophene plane was almost perpendicular to the first thiophene plane.

In the second step, the co-adsorption complex of **MIN-1** passes through a transition state **TS-1** and forms an intermediate **MIN-2**. This step is indeed an electrophilic aromatic substitution. At first, the adsorbed thiophene molecule is protonated by the zeolite proton (H1 at O2) at its α-site (C1). This protonated thiophene immediately attacks the second thiophene molecule at its α-site (C5), finally producing 2-(2,5-dihydrothiophen-2-yl) thiophene and restoring the Brønsted acid site by transferring H2 at C5 back to O2. The reaction barrier is 143.1 kJ/mol. Because the protonation and thiophene dimerization steps occur simultaneously, no protonated thiophene intermediate can be found. It has been shown that only bulky carbocations can be observed experimentally within the zeolite pore [41,42].

In **TS-1**, the C1–H1 had a length of 1.09 Å, and the distances of H1 to O2 and O1 were 2.66 and 2.59 Å, respectively. The distance of C4 and C5 coupling was 1.99 Å, and H2 at C5 directing to O2 had a distance of 1.90 Å. In **MIN-2**, the regenerated acidic proton (H2) directed to S1 with a distance of 2.14 Å, enabling further protonation and ring-opening.

The cleavage of the C–S bond between S1 and C4 was achieved through a transition state **TS-2** from **MIN-2**, result-

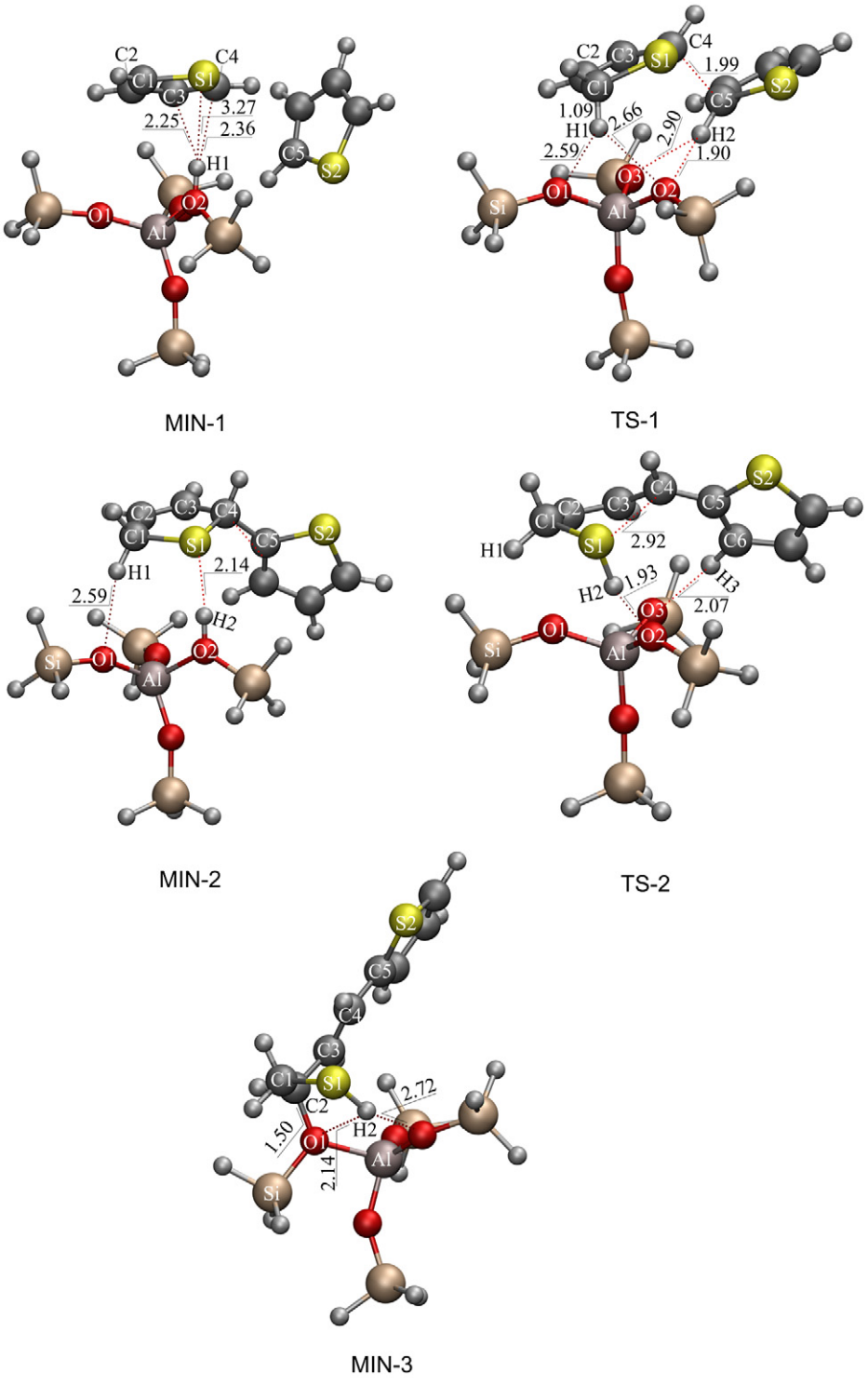

Fig. 3. Structures of stationary points in path 1 with selected parameters optimized at the B3LYP/6-311G(d,p) level.

ing in 4-mercapto-1-(thiophen-2-yl)but-2-en-1-ylium intermediate **MIN-3**. The activation barrier for this process was only 103.1 kJ/mol, 40.0 kJ/mol lower than that of the first step (143.1 kJ/mol). In addition, the cleavage of S1–C1 bond was also possible, but the computed energy barrier of 204.0 kJ/mol was much higher than that of S1–C4; therefore, the cleavage of S1–C1 bond was not competitive. For comparison, we also computed the C–S bond-cracking barrier proposed by Saintigny et al. [16] using the same model and the same method. The calculated barrier was 287 kJ/mol, much higher than our value (103.1 kcal/mol). Such a large energy difference can be attributed to the stabilizing effect of TS-2 by the second thiophene ring.

It is notable that intermediate **MIN-3** contained CH_2 fragments close to a double bond or to a sulfur atom, in agreement with the experimental results. It is also noteworthy that **MIN-3**

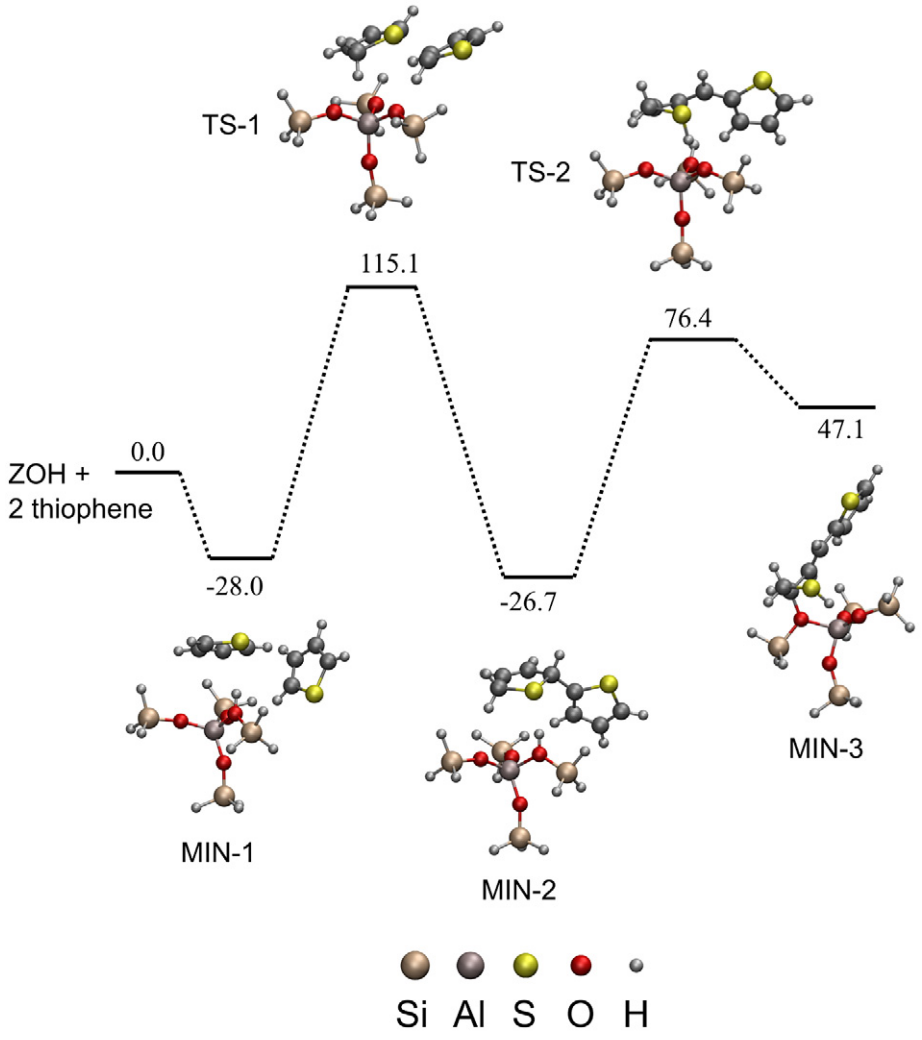

Fig. 4. Energy profile of 5T cluster and the relative energies (kJ/mol) calculated at B3LYP/6-311 + G(2d,p)//B3LYP/6-311G(d,p) + ZPE (B3LYP/6-311G(d,p)).

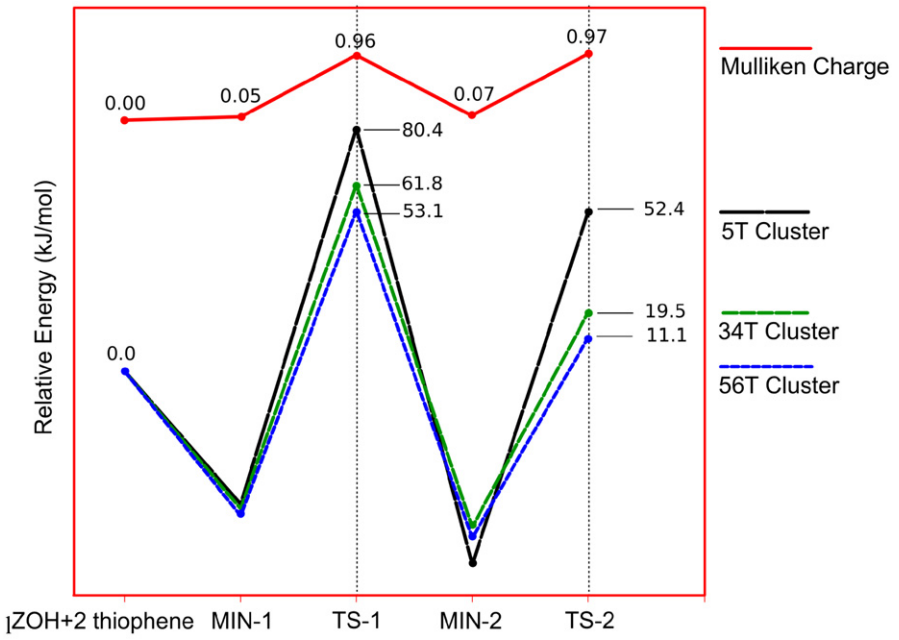

Fig. 5. 5T, 34T and 56T energy evolution (the given charge is the total charge only on the adsorbate).

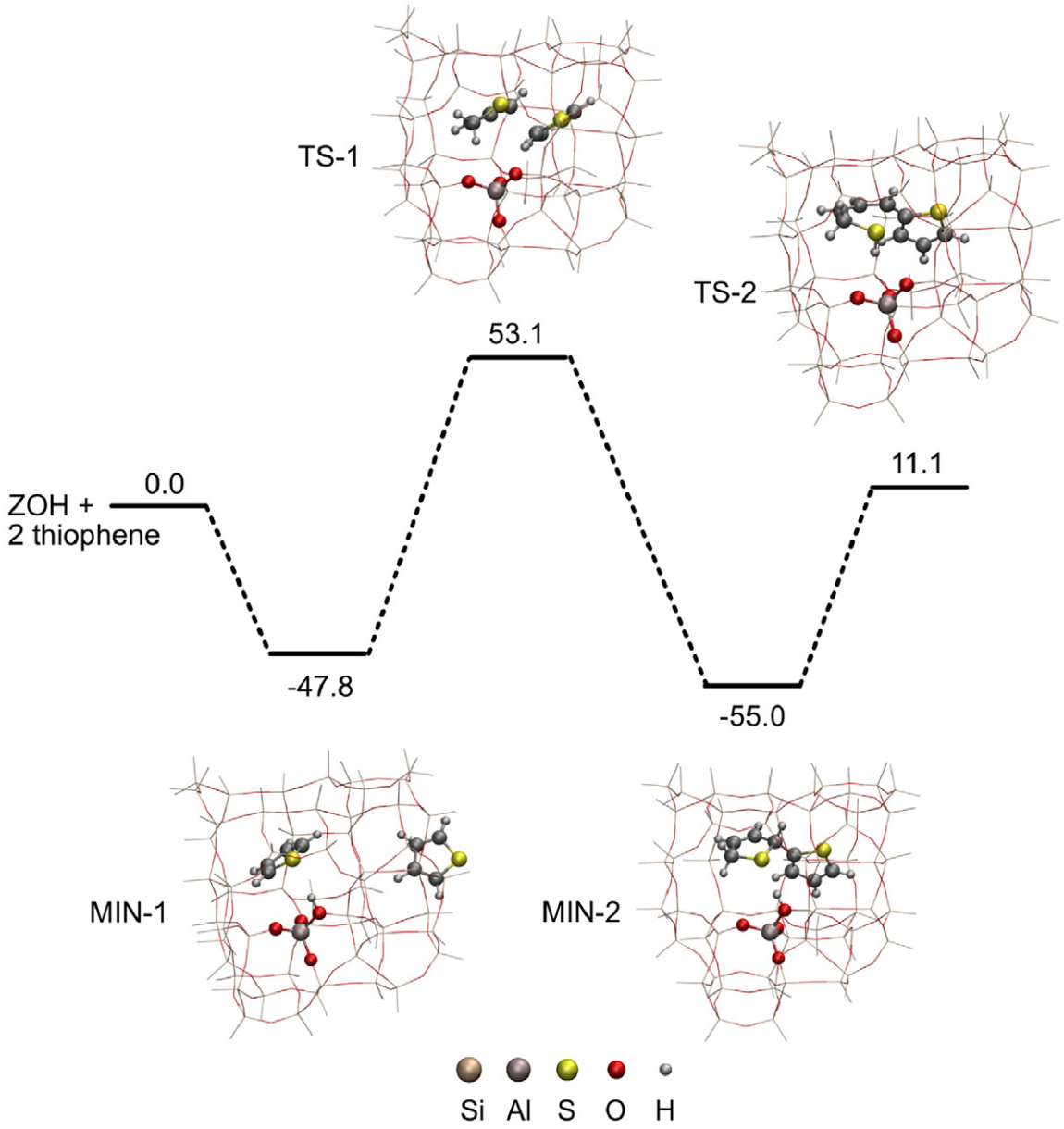

Fig. 6. Reaction coordinate for thiophene cracking over 56T cluster (kJ/mol, at B3LYP/6-31G(d)).

can be considered to be the chemisorbed state of the intermediate C in Scheme 3, which is similar to the intermediate A in Scheme 2 proposed by Shan et al. However, our mechanism for obtaining intermediate A differs from that shown in Scheme 2.

3.2. Influence of zeolite framework on the activation energies for thiophene cracking

It is well known that zeolite structures play an important role in stabilizing carbonium ion and positively charged transition states, and that the more positively charged the transition state, the stronger the stabilization effects. This stabilization effect can be achieved only by long-range and electrostatic interaction between the adsorbates and the zeolite framework. In our **5T** cluster, both **TS-1** and **TS-2** were positively charged due to the proton transfer; therefore, a strong stabilization effect by the zeolite framework should be expected. To demonstrate this effect, we used the embedded 34T and 56T clusters, as described in Section 2, and the computed results are summarized in Figs. 5 and 6.

As shown in Fig. 5, the adsorbed thiophene derivatives in **MIN-1** and **MIN-2** were neutral (0.05e and 0.07e Mulliken charge, respectively), whereas **TS-1** and **TS-2** were positively charged (0.96e and 0.97e Mulliken charge, respectively). Therefore, both **TS-1** and **TS-2** should have had a greater stabilization effect in the **34T** and **56T** clusters. The stabilization effect of **MIN-1** and **MIN-2** from **5T** to **34T** and **56T** was rather small, whereas that of **TS-1** and **TS-2** from **5T** to **34T** and **56T** was very large (Table 1). In **TS-1**, the stabilization effects from **5T** to **34T** and **56T** were −18.6 and −27.3 kJ/mol, respectively. The most pronounced stabilization

effect was found for **TS-2** from **5T** to **34T** and to **56T** by −32.9 and −41.3 kJ/mol, respectively. The result was lowered reaction barriers (Fig. 6).

Comparing our results with those in the literature yields some interesting findings. As discussed earlier, the previously calculated barriers for C–S bond-cracking of 222–318 kJ/mol are too high, considering that C–S bond has a average strength of about 290 kJ/mol and that thiophene cracking can occur at ambient temperatures. In contrast, our proposed barrier of about 101 kJ/mol is much lower than the literature values and is reasonable based on the experimental findings. Also note that the intermediate in our mechanism has a CH_2 group close to the C=C double bond and the SH group, in agreement with the experimental findings.

4. Conclusion

We have proposed a new mechanism for thiophene cracking catalyzed by Brønsted acidic zeolite on the basis of B3LYP DFT calculations. Based on a **5T** cluster model, a second thiophene molecule was found to be necessary to promote the catalytic reaction. Our proposed mechanism involves two major steps. The first step is the protonation of the α site of thiophene close to the acidic center, followed by an electrophilic aromatic substitution to the second thiophene molecule and regeneration of the acidic center on zeolite in a concerted way; this step forms 2-(2,5-dihydrothiophen-2-yl) thiophene as the first intermediate. The second step is the protonation of the sulfur center in the 2,5-dihydrothiophene moiety, followed by the simultaneous C–S bond dissociation; this step results in formation of the second intermediate, 4-mercapto-1-(thiophen-2-yl)but-2-en-1-ylium.

A strong stabilization effect of the zeolite framework was demonstrated by embedding the 5T cluster into the larger **34T** and **56T** clusters. The long-range and electrostatic interactions strongly stabilize the two transition states and lower the corresponding barriers. The rate-determining step is electrophilic aromatic substitution (101 kJ/mol), whereas the subsequent C–S bond dissociation has a lower barrier (66 kJ/mol). Our results agree reasonably with the experiments: The intermediate, 4-mercapto-1-(thiophen-2-yl)-but-2-en-1-ylium, has a CH_2 group close to a C=C double bond and a SH group, and the estimated barrier of 101 kJ/mol explains the fact that such catalytic reactions can occur at room temperature.

Acknowledgments

Financial support was provided by the National Basic Research Program of China (2004CB217802) and National Natural Science Foundation of China (20403028).

Supporting information

Optimized structures for all 5T clusters; total electronic energies for all 5T, 34T and 56T clusters; thiophene protonation energies; and reaction coordinate figure for thiophene cracking path-2 over 5T cluster are summarized in supporting information.

Please visit DOI: 10.1016/j.jcat.2007.10.006.

References

[1] T.G. Albro, P.A. Dreifuss, R.F. Wormsbecher, J. High Res. Chromatogr. 16 (1993) 13.
[2] W.C. Cheng, G. Kim, A.W. Peters, X. Zhao, K. Rajagopalan, M.S. Ziebarth, C.J. Pereira, Catal. Rev.-Sci. Eng. 40 (1998) 39.
[3] C. Yin, G. Zhu, D. Xia, Am. Chem. Soc. Prepr. Div. Pet. Chem. 47 (2002) 391.
[4] C. Yin, G. Zhu, D. Xia, Am. Chem. Soc. Prepr. Div. Pet. Chem. 47 (2002) 398.
[5] M. Landau, D. Berger, M. Herskowitz, J. Catal. 158 (1996) 236.
[6] M. Landau, Catal. Today 36 (1997) 393.
[7] P. Michaud, J. Lemberton, G. Perot, Appl. Catal. A 169 (1998) 343.
[8] C.L. Garcia, J.A. Lercher, J. Phys. Chem. 96 (1992) 2669.
[9] C.L. Garcia, J.A. Lercher, J. Mol. Struct. 293 (1993) 235.
[10] W.J.J. Welters, G. Vorbeck, H.W. Zandbergen, J.W. Dehaan, V.H.J. Debeer, R.A. Van Santen, J. Catal. 150 (1994) 155.
[11] S.Y. Yu, W. Li, E. Iglesia, J. Catal. 187 (1999) 257.
[12] S.Y. Yu, J. Garcia-Martinez, W. Li, G.D. Meitznerb, E. Iglesia, Phys. Chem. Chem. Phys. 4 (2002) 1241.
[13] W.J.J. Welters, V.H.J. de Beer, R.A. van Santen, Appl. Catal. A 119 (1994) 253.
[14] B.A. De Angelis, G. Appierto, J. Colloid Interface Sci. 53 (1975) 14.
[15] L.J. Simon, M. Rep, J.G. van Ommen, J.A. Lercher, Appl. Catal. A 218 (2001) 161.
[16] X. Saintigny, R.A. van Santen, S. Clémendot, F. Hutschka, J. Catal. 183 (1999) 107.
[17] X. Rozanska, R.A. van Santen, F. Hutschka, J. Catal. 200 (2001) 79.
[18] X. Rozanska, R.A. van Santen, F. Hutschka, J. Hafner, J. Catal. 215 (2003) 20.
[19] H.H. Shan, C.Y. Li, C.H. Yang, H. Zhao, B.Y. Zhao, J.F. Zhang, Catal. Today 77 (2002) 117.
[20] D.G. Aksenov, O.V. Klimov, G.V. Echevskii, E.A. Paukshtis, A.A. Budneva, React. Kinet. Catal. Lett. 83 (2004) 187.
[21] A. Chica, K. Strohmaier, E. Iglesia, Langmuir 20 (2004) 10982.
[22] A. Chica, K. Strohmaier, E. Iglesia, Appl. Catal. B 60 (2005) 223.
[23] A.D. Becke, J. Chem. Phys. 98 (1993) 5648.
[24] C. Lee, G. Yang, R.G. Parr, Phys. Rev. B 37 (1988) 785.
[25] S.A. Zygmunt, R.M. Mueller, L.A. Curtiss, L.E. Iton, J. Mol. Struct. (THEOCHEM) 4309 (1998) 430.
[26] M.P. Andersson, P. Uvdal, J. Phys. Chem. A 109 (2005) 2937.
[27] M.J. Frisch, G.W. Trucks, H.B. Schlegel, G.E. Scuseria, M.A. Robb, J.R. Cheeseman, J.A. Montgomery Jr., T. Vreven, K.N. Kudin, J.C. Burant, J.M. Millam, S.S. Iyengar, J. Tomasi, V. Barone, B. Mennucci, M. Cossi, G. Scalmani, N. Rega, G.A. Petersson, H. Nakatsuji, M. Hada, M. Ehara, K. Toyota, R. Fukuda, J. Hasegawa, M. Ishida, T. Nakajima, Y. Honda, O. Kitao, H. Nakai, M. Klene, X. Li, J.E. Knox, H.P. Hratchian, J.B. Cross, V. Bakken, C. Adamo, J. Jaramillo, R. Gomperts, R.E. Stratmann, O. Yazyev, A.J. Austin, R. Cammi, C. Pomelli, J.W. Ochterski, P.Y. Ayala, K. Morokuma, G.A. Voth, P. Salvador, J.J. Dannenberg, V.G. Zakrzewski, S. Dapprich, A.D. Daniels, M.C. Strain, O. Farkas, D.K. Malick, A.D. Rabuck, K. Raghavachari, J.B. Foresman, J.V. Ortiz, Q. Cui, A.G. Baboul, S. Clifford, J. Cioslowski, B.B. Stefanov, G. Liu, A. Liashenko, P. Piskorz, I. Komaromi, R.L. Martin, D.J. Fox, T. Keith, M.A. Al-Laham, C.Y. Peng, A. Nanayakkara, M. Challacombe, P.M.W. Gill, B. Johnson, W. Chen, M.W. Wong, C. Gonzalez, J.A. Pople, Gaussian 03 (Revision B.04), Gaussian, Inc., Pittsburgh, PA, 2003.
[28] W. Humphrey, A. Dalke, K. Schulten, J. Mol. Graph. 14 (1996) 33.
[29] S.A. Zygmunt, L.A. Curtiss, P. Zapol, L.E. Iton, J. Phys. Chem. B 104 (2000) 1944.
[30] H. van Koningsveld, H. van Bekkum, J.C. Jansen, Acta Crystallogr. B 43 (1987) 127.

[31] E.G. Derouane, J.G. Fripiat, Zeolites 5 (1985) 165.
[32] A.E. Alvarado-Swaisgood, M.K. Barr, P.J. Hay, A. Redondo, J. Phys. Chem. 95 (1991) 10031.
[33] K.P. Schröder, J. Sauer, M. Leslie, C. Richard, A. Catlow, Zeolites 12 (1992) 20.
[34] S. Yuan, J. Wang, Y.-W. Li, S. Peng, J. Mol. Catal. A 178 (2002) 277.
[35] S. Yuan, J. Wang, Y.-W. Li, H. Jiao, J. Phys. Chem. A 106 (2002) 8167.
[36] S. Yuan, W. Shi, B. Li, J. Wang, H. Jiao, Y.W. Li, J. Phys. Chem. A 109 (2005) 2594.
[37] S. Yuan, J. Wang, Y.W. Li, H. Jiao, J. Nat. Gas Chem. 12 (2003) 93.
[38] C. Tuma, J. Sauer, J. Chem. Phys. Lett. 387 (2004) 388.
[39] J. Sauer, M. Sierka, F. Haase, in: D.G. Truhlar, K. Morokuma (Eds.), Transition State Modeling for Catalysis, in: ACS Symp. Ser., vol. 721, Am. Chem. Soc., Washington, 1999, p. 358.
[40] T. Baba, N. Komatsu, Y. Ono, H. Sugisawa, J. Phys. Chem. B 102 (1998) 804.
[41] J.F. Haw, J.B. Nicholas, T. Xu, L.W. Beck, D.B. Ferguson, Acc. Cem. Res. 29 (1996) 259.
[42] T. Xu, J.F. Haw, J. Am. Chem. Soc. 116 (1994) 7753.